ACS APPLIED MATERIALS & INTERFACES

Research Article

www.acsami.org

Dispersed, Porous Nanoislands Landing on Stretchable Nanocrack Gold Films: Maintenance of Stretchability and Controllable Impedance

Zhiyuan Liu,‡ Mei Yu,‡ Junhui Lv, Yuchun Li, and Zhe Yu*

Biomedical Microdevices Research Laboratory, Shenzhen Institutes of Advanced Technology, Chinese Academy of Sciences, 1068 Xueyuan Avenue, Shenzhen 518055, China

Supporting Information

ABSTRACT: Stretchable electronic devices have great potential for serving as bioelectrical interfaces due to their better deformability and modulus match with biological organs. However, surface modification, which is usually applied to enhance the capability of sensing and stimulating, as well as biocompatibility, may cause problems since their stretchability highly depends on the surface structure. In this work, stretchable nanocrack gold (SNCG) electrodes were fabricated, which can be stretched by a maximum 120% uniaxial strain while maintaining their electrical conductivity. We found that the electrodes lost their stretchability after surface modification of an additional continuous platinum layer, which was found to selectively weld or fully cover the nanocracks, consequently eliminating its crack structure. To address this issue, we designed a complex structure of dispersed, porous nanoislands landing on the SNCG film, which was further demonstrated as capable of maintaining the stretchability of electrodes while allowing the reshaping of cracks. Moreover, stretchable microelectrode arrays were then developed with this complex structure. Animal experiments demonstrated their capability of conformally wrapping on a rat brain cortex and effectively monitoring an intracranial electroencephalogram under deformation. In addition, their impedance can be precisely controlled by modulating the dispersity, diameter, and aspect ratio of individual nanoislands. This complex structure has great potential for developing highly stretchable, multiplexing sensors, allowing stiff materials to land on a stretchable conducting surface with maintenance of stretchability and controllable functional area.

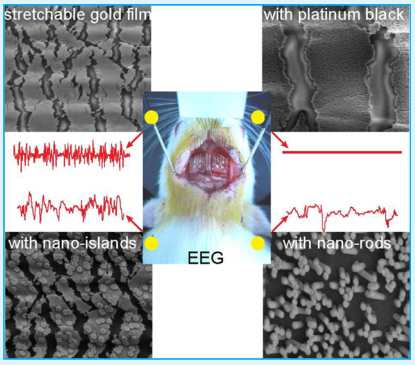

KEYWORDS: *stretchable electronics, stretchable gold film, nanoisland, surface modification, intracranial electroencephalogram*

1. INTRODUCTION

Micro- and nanoelectrode arrays (M/NEAs), which are capable of monitoring and modulating biological activity at high spatial resolution *in vivo*, create links for communications between electronic devices and biological systems. Although they have been widely used for clinical diagnosis and treatment of diseases, and for intelligent control,[1−3] it is still challenging for the implantable devices to intimately contact the supple and curved target tissues while causing little damage. When directly contacting biological tissues and organs, the devices need to physically and functionally match with the biological targets to realize communications with biological systems. However, the mismatch strain at the interface between rigid devices and biological tissues may inevitably generate tissue damage, scarring, as well as the failure of the devices, causing problems for long-term implantation.[4] Stretchable electronic devices have been researched and developed intensively during the past decade due to their robust mechanical and electrical properties.[5−7] The devices are usually made from gold,[8−11] semiconductors,[12] conducting polymers,[13] graphene,[14] and nanowires[15] on stretchable substrates based on the principle of designing a geometrical pattern of conductors,[16] introducing micro/nano-crack structures to metal films,[10,17] or doping metal ions, particles, and composite materials into stretchable substrates,[18−20] among which the stretchable gold film is one of the most promising technologies for biomedical applications due to its better modulus match, deformability, and biocompatibility.[5,21,22] Stretchable microelectrode arrays fabricated with stretchable gold films can be curved, twisted, and even reshaped with biological organs and tissues while maintaining robust electrical properties; therefore they hold great promise for solving the stress concentration problems.[5,21,23]

Although gold has great electrical conductivity, its charge transfer capability is relatively low compared to platinum and iridium. Moreover, an electrical double layer appears on the surface of the gold electrode when it is immersed in electrolyte solutions (e.g., body fluids). As the size of electrodes reaches to micron scale, the double-layer impedance of the gold electrode rapidly increases, and as a result, its capability of detecting tiny

Received: April 24, 2014
Accepted: August 4, 2014
Published: August 4, 2014

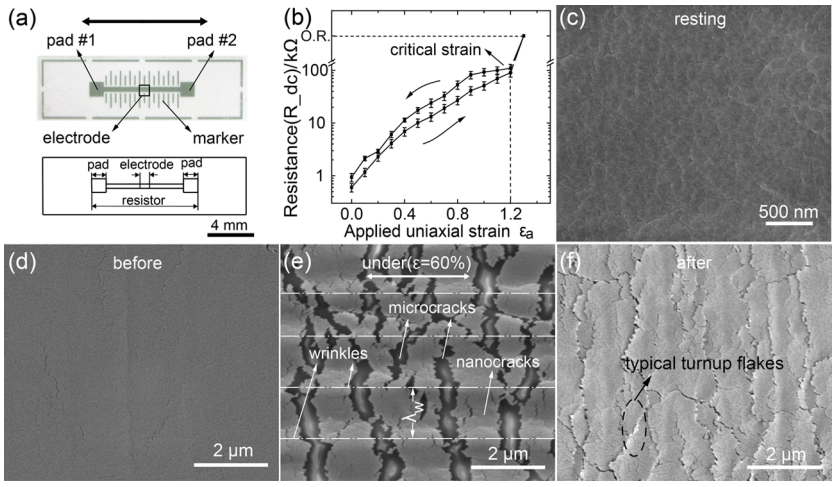

Figure 1. An SNCG sample and its structures and electrical properties. (a) Optical image and cartoon illustration of the sample, which consists of connecting pad #1 and #2, an electrode, and a scale marker for positioning the encapsulation layer. Detailed structures are described in the Supporting Information. The black double arrow line shows the direction for the uniaxial stretch. (b) Resistance of SNCG samples while they are stretched at different applied uniaxial strains (n = 5), where O.R. represents that the resistance is out of measuring range, indicating a fracture of the sample. (c) SEM image of an SNCG film at the resting state. The mean length of nanocracks is 90 ± 8 nm (mean ± S.D., n = 100) with random orientations. (d–f) SEM images of an SNCG film before, under, and after stretching. The typical structures of cracks, wrinkles, wrinkle wavelength, λ_w, and turnup flakes are marked with white arrows. The white double arrow line in e shows the direction for the uniaxial stretch.

biological signals will dramatically decrease, or even be eliminated, due to a poor signal-to-noise ratio (SNR). Therefore, surface modification is vital for reducing the input impedance of the electrode and thus increasing SNR. There have been many existing methods for electrode surface modification by using the materials with high charge transfer capability, such as platinum,[24] Pt–Ir,[25] and IrO_2,[26] and forming rough or porous topographies to enlarge effective surface area of the electrode, such as nanoflakes,[27] nanorods,[28] and nanotubes.[29] Besides these stiff and brittle materials, soft materials, such as conducting polymers with various dopings[30−32] and multiple layers of PPy and CNTs,[33] have been used to modify the electrode surface for better biocompatibility. However, little work has been specifically done on the surface modification for stretchable electrodes and how the modification affects their conductivity and stretchability, which could be crucial for the functionality of stretchable electronic devices because the stretchability of stretchable gold films highly depends on the morphology and structure of the electrode surface.

Up to now, there has been little research investigating the surface modification methods for stretchable electronic devices or their impacts on their stretchability and other properties. In this study, stretchable electrodes are designed and fabricated based on the technology of stretchable gold films with nanocracks, which enables the electrodes to keep conducting while being stretched at large uniaxial strains. The surface modification of an additional platinum layer on electrodes is implemented, and its effect on the performance of stretchable electrodes is evaluated. The stretchability of stretchable nanocrack gold (SNCG) films is found significantly reduced and even eliminated by the surface modification, and the mechanisms underlying this phenomenon are investigated. To address this issue, we then propose a complex structure of dispersed, porous nanoislands landing on SNCG films, which is designed to be compatible with the nanocrack structure of SNCG films to maintain their stretchability, and meanwhile have a controllable, large effective surface area to reduce the electrode impedance.

2. RESULTS AND DISCUSSION

A typical SNCG sample designed for this study is shown in Figure 1a. A detailed fabrication process (Figure S1 in the Supporting Information) and the conductor structure are described in the Experimental Procedures. We fabricate stretchable gold films with nanocracks on the substrate of polydimethylsiloxane (PDMS; Figure 1a). The critical uniaxial strain or the maximum uniaxial strain while the gold film maintains conduction, characterized as stretchability of the gold film, can reach as high as about 120% (see Figure 1b and the Supporting Information for details). Herein, the resistance out of the measuring range (O.R., i.e. beyond 40 MΩ) indicates functional rupture of the film conductor, and the strains where the resistance is O.R. are defined as electrical rupture strains, at which the sample is still mechanically robust (see Figure S2 in the Supporting Information). A customized stretcher device is designed for stretching the electrode at a certain amount of strain and for scanning electron microscope (SEM, NOVA NanoSEM 450, FEI) imaging while the electrode is being stretched (see Figure S3c in the Supporting Information). Initial nanocracks can be found in the film uniformly distributed with random orientation (Figure 1c), and the mean length of nanocracks is 90 ± 8 nm (mean ± S.D., n = 100). While the SNCG film is being stretched for the first time, some of the initial nanocracks propagate and coalesce into large microscale cracks to ease local stress; simultaneously, wrinkles appear due to the mismatch of elastic moduli and Poisson's ratio between the gold film and the PDMS substrate (Figure 1e), similar to what happens to a paper-cut pattern while it is being stretched (see Figures S3a,b in the Supporting Information).

Resistance between the two testing contact pads (Figure 1a) is measured before, under, and after stretching, tracking the change of conductivity and the critical strain of electrodes. The SNCG sample is uniaxially stretched up to the critical strain and

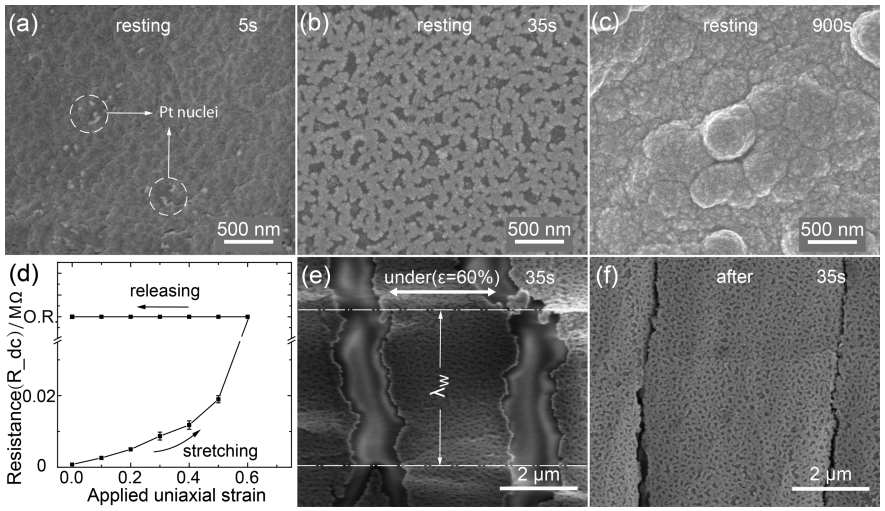

Figure 2. Growth process of DED platinum black on a SNCG electrode and its electrical and mechanical properties. (a–c) SEM images of the modified electrode with different quantity of platinum at the resting state, indicated by the electrodeposition duration at the current density of 3 mA/cm^2. (d) Resistance of sample b while it is stretched at different uniaxial strains, where O.R. represents that the resistance is out of the measuring range. (e,f) SEM images of the sample b under a stretch of 60% strain and after it is fully relaxed. The white double arrow line in e shows the direction for the uniaxial stretch, and the wrinkle wavelength, λ_w, is marked between the white dash dot lines.

then relaxed, gradually. The resistance at each static strain is measured (between pad #1 and pad #2 in Figure 1a). Multiple samples are tested, and the critical strain value of 120% is highly repeatable, indicating its intrinsic property of the SNCG film (Figure 1b and Figure S3d in the Supporting Information). Moreover, the increase in the resistance under deformation is reversible, and the resistance versus the applied strain shows a hysteresis curve (also reported by other groups[5,34]). Some of the initial nanocracks in the SNCG film propagate and coalesce into large microscale cracks during the first stretch, and then the large microcracks open and close when the film is stretched thereafter (Figure 1e). The resistance after being fully relaxed is slightly higher than that before stretching (Figure 1b) because of the contact resistance between the two edges of cracks when the cracks close. The AC impedance of electrodes (between pad #1 and the electrode in Figure 1a) under deformation is examined as well, when the electrode is immersed in phosphate-buffered saline (PBS, pH = 7.4), which is a commonly used physiological saline with the same osmolarity as human blood. This impedance along the direction of stretch is different from that perpendicular to it,[35] due to the selected orientation of the cracks generated through uniaxially stretching (Figure 1e). Herein, the total impedance $Z = R_{dc} + Z_{dl}$, where R_{dc} represents the DC resistance of the conducting wire between pad #1 and the electrode; Z_{dl} represents the impedance mainly from the double layer capacitance on the surface. The R_{dc} is usually ignorable comparing with Z_{dl} at the resting status; however, as the electrode is being stretched, the value of R_{dc} may dramatically rise and even dominate. The electrode impedance under deformation at high frequency (e.g., 10 kHz) performs similarly to the DC resistance due to the domination of the DC component. Differently, at as low a frequency as 1 Hz, the AC impedance has no character of hysteresis but decreases with the increase of the applied strain (Figure S3e in the Supporting Information) which is most likely ascribed to the increase of effective surface area caused by the detachment of the SNCG film under stretching,[36] which turns out to be the out-of-plane flakes as shown in Figure 1f when the film is fully relaxed.

The mechanisms underlying the mechano-electrical behaviors of stretchable gold films were previously investigated, and the release of strain energy by deflecting and twisting out of plane[17] and alteration of the conducting percolation path in the presence of Poisson's ratio[37] were proposed to interpret the stretchability of stretchable gold films. In this study, we investigate the SEM images of SNCG films under stretching and find that the composite structure of cracks and transverse wrinkles as shown in Figure 1e may perform crucial importance in contributing to the stretchability of SNCG films. The stretchable electrode keeps conducting under as large as 120% uniaxial strain, and although its resistance increases along with stretching, the changes in electrode resistance are reversible. However, an additional layer for surface modification on the stretchable electrode may eliminate the initial nanocracks. As a result, the critical strain may decrease even to zero, and the film cannot keep being conductive while being stretched any more, indicating a loss of stretchability.

Electrodepositing platinum black (PB) is one of the most widely used materials for electrode modification because of its inherent high charge transfer capability of platinum and the large effective area due to its porous structure.[38] In this work, direct electrodeposited (DED) platinum, which is widely used for electrode surface modification,[39] is applied for surface modification of the SNCG electrodes, and the applied current density and duration for electroplating are optimized and evaluated further while the electrodes are under no strain (see Figure S4 in the Supporting Information). A moderate current density (3 mA cm^{-2}), DED 3-35, is applied for preparing the samples for platinum electrodeposition in the following study. As the quantity of exchanging charge reaches around 0.5 mC (3 mA cm^{-2} for 35 s with the electrode surface area of 0.5 mm^2), defined as DED 3-35, the impedance decreases rapidly to a typical or target level, at which a microelectrode with an active area of 10 μm × 10 μm has an impedance of about 1 MΩ at 1 kHz, a value less than what is required to ensure a reasonable SNR for sensing tiny biological signals. Although the microelectrode of 10 μm × 10 μm is not prepared in this study, an appropriate method for surface modification is

important to guarantee its capability of monitoring bioelectrical activity for future studies as needed.

The electrodeposition process of platinum on the SNCG electrode surface is investigated first, which involves of progressive nucleation and growth. The formation of nuclei on the electrode surface during electrodeposition has been considerably studied and is generally believed to be influenced by the surface energy and crystal structure of the electrode, based on thermodynamics. However, in the presence of the nanocracks on the SNCG electrode surface, the platinum nuclei are found appearing initially on the edges and tips of cracks due to the nonuniform distribution of the electric field (Figure 2a). After that, a number of nuclei gradually grow along the cracks and then overlap and form cross-linked stripes covering the cracks (Figure 2b). Although the cracks are vital for the stretchability, they are first plated and gradually lose their contribution to the stretchability. Finally, the platinum keeps growing into a continuous platinum film and covers all over the electrode surface with the initial nanocracks eliminated (Figure 2c).

As shown in Figure 2b, DED 3−35 represents a status, in which the platinum forms cross-linked stripes, covering cracks but not all over the electrode surface. The electrical properties of the modified electrode at different uniaxial strains are investigated. The resistance results show that the critical strain of the modified electrode (during the first stretching after the modification) decreases from 110% to 50% after the modification. And even more serious is that the increases in electrode resistance during stretching is not reversible any more, and the electrode never returns to being conductive after entire relaxation (Figure 2d). These results demonstrate that the stretchable electrode totally loses its stretchability after the modification, indicating a fracture of the electrode (Figures 2e,f). Additionally, if the samples are applied with the maximum strain of 40%, less than the critical strain, the electrical resistance still keeps the characteristic of hysteresis for DED 3-5 and 3-35, but the DED 3-900 sample loses its conductivity immediately when applied with a small strain, indicating that it loses its stretchability completely (Figure S5 in the Supporting Information).

The electrodeposited platinum layer changes the crack structure of the SNCG film after the surface modification, leading to the loss of its stretchability. After the surface modification, the platinum prefers to grow along the cracks first and forms cross-linked stripes covering the cracks during the electrodeposition process. As a result, most of the initial nanocracks are welded (Figure 2b), and they are not capable of self-organized growth and combination to release stress. Besides the elimination of nanocracks, the transverse wrinkles are restrained after the surface modification. Figure 2e shows that the transverse wrinkle wavelength is about 4 μm (Figure 2e), larger than the 1.3 μm before modification (Figure 1e). According to the principle of system energy minimum, when the substrate is relatively thick, the wavelength of the wrinkles is as following:[40]

$$\lambda_w = 2\pi h_f \left(\frac{\bar{E}_f}{3\bar{E}_s} \right)^{1/3} \quad (1)$$

where $\bar{E}_s = E_s/(1 - \nu_s^2)$, $\bar{E}_f = E_f/(1 - \nu_f^2)$ are the plane strain moduli and E_s, ν_s, E_f, and ν_f are the substrate and film's elastic modulus and Poisson's ratio, respectively; the subscripts s and f represent the substrate and the film; h_f is the thickness of the film. Obviously, the increases of the film thickness, h_f, and the film plane strain modulus, $\bar{E}_f$, after the surface modification, both suppress transverse wrinkles, thus increasing the wavelength. Taken together, the surface modification of DED platinum eliminates the crack structure and suppresses transverse wrinkles, and as a result, the stretchability of the SNCG electrode is tampered or even destroyed.

Most modification materials, including conducting polymers, are not stretchable or have as poor stretchability as less than 5%.[1] Therefore, particular structures and morphologies of the modification layer are needed to preserve the stretchability of the electrodes. Rather than finding and applying an ideal modification layer with high charge transfer capability and large stretchability, we design and modify the stretchable electrode with a complex structure of dispersed, porous platinum nanoislands, which maintains the high charge transfer capability of platinum and also possesses a controllable, large effective area. More importantly, the layer of the dispersed nanoislands to some extent resembles the nanocracks structure. Currently, advanced nanostructures and nanomaterials of nanorods and nanowires have been developed with precise control of morphology, structure, and composition on multiple length scales.[41,42] Given the advantage of these nanotechnologies, the complex structure of dispersed nanoislands landing on a conducting SNCG film has great potential for developing novel highly stretchable, multiplexing, and multifunctional sensors.

In this study, the dispersed nanoislands are fabricated by using the template-assisted electrodeposition (TAED). The track-etched polycarbonate (PC) film is used as a template to prepare platinum nanoislands by allowing the deposition of platinum into the channels or cylindrical pores within it (Figure 3a−c). Compared with the methods for growing solid

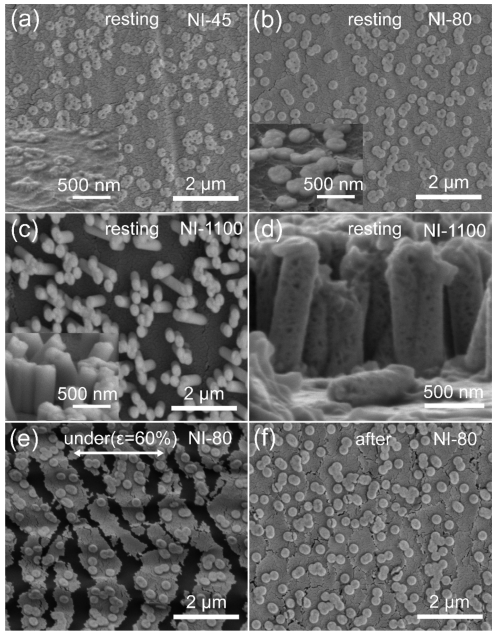

Figure 3. SEM images of dispersed, porous nanoislands landing on SNCG films. (a-d) SEM images of nanoislands with different heights. Insets in (a), (b) and (c) show SEM images from 60°-view, and image in (c) from 90°-view is shown in (d). (e-f) SEM images of NI-80 under and after stretch. NI-80 has almost the same impedance performance as PB (DED 3−35). The white double arrow line in (e) shows the direction for the uniaxial stretch.

nanostructures, the TAED process is able to fabricate similar porous features as the DED process (Figure 3d), which provides more active area inside the nanostructures. A PC membrane (Isopore, Millipore) with a porosity of 25% and pore size of 200 nm is attached to the film, and after encapsulation, the current density of 3 mA/cm^2 is applied for 140 s, 260 s, and 3600 s (TAED 3−3600) to deposit nanoislands with different heights of 45 nm, 80 nm, and 1.1 μm (NI-45, NI-80, and NI-1100), respectively (Figure 3a−c). The PC membrane is then removed with Remover PG (MicroChem) after the deposition. Given the PC membrane with 25% porosity on top, the active area for the TAED process is about one-quarter of that for the DED process. Therefore, the total amount of the deposited platinum for the previous Pt-black structure (DED 3-35) is roughly the same as that for the nanoislands structure with a height of 45 nm (TAED 3-140). However, despite the same quantity of platinum, the equivalent capacitance per area of the NI-45 modified electrodes, which is defined as the capacitance divided by the original electrode surface area before the modification, is lower than that of the PB (DED 3−35) modified electrodes (Figure 4a, using Levenberg−Marquardt method[43]), due to the relative decrease in the effective area of platinum.

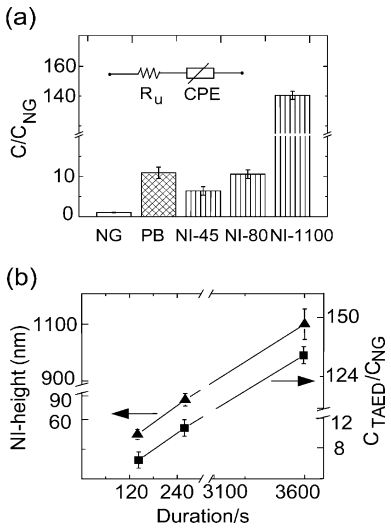

Figure 4. Controllable impedance performance. (a) The equivalent capacitance per area of the NG, PB (DED 3-35), NI-45, NI-80, and NI-1100 electrode samples. The values are normalized by that of NG. The inset shows the fitting CPE model using the Levenberg−Marquardt method. (b) Linear relationship between the electrodeposition duration and the height of the nanoisland (left ordinate) and the normalized equivalent capacitance per area (right ordinate).

Although the deposition is restrained within the pores, total effective platinum area can be controllable and increased to even more than the electrode surface area by elongating the nanoislands to nanorods or nanowires, which are usually distinguished according to their aspect ratios, and can be achieved simply by applying different plating times (Figure 3a−c). As shown in Figure 4a, the NI-80 modified electrodes have comparable capacitance per area with the PB (DED 3-35) modified ones and have a similar crack structure with naked gold (NG) film under and after stretching (Figure 3e,f). Furthermore, a 12 times larger capacitance per area than that of the PB (DED 3-35) modified electrodes can be achieved when the nanoislands grow into nanorods with a height of about 1.1 μm (NI-1100), as shown in Figures 3c and 4a. Different from the DED method, by which the capacitance per area tends to be saturated (see Figure S4 in the Supporting Information) after the electrode surface is fully covered by platinum (see DED 3-900 in Figure 2c, which has the same quantity of platinum as the TAED 3-3600) since the increased platinum lays over the previous layer and contributes little to the increase of the total effective area, the TAED method allows nanoislands unlimited growth out of plane rather than in-plane, and the total effective area can be increased linearly by extending nanoislands, and there is no leveling off observed in this work (Figure 4b and see theoretical explanation in the Supporting Information), indicating that this method can make the impedance continuously decrease by plating through pores.

Although the dispersed platinum nanoislands cover about 25% of the surface area, they allow the crack structure to appear and grow during stretching because the nanoislands are dispersed and isolated. The modification of the nanoislands, to some extent, reduces the number and dispersity of the cracks by around 25%, which tampers with the crack structure. However, the stretchability of the modified electrodes is well maintained despite some decrease. The dynamic process of the crack expansion for NI-80 and DED3-35 during stretching is shown in detail in the Supporting Information. As shown in Figure 5a, although the critical strain of the stretchable electrodes modified with NI-45 and NI-80 is around 80%, decreasing from 120% for NG electrodes, the resistance fully recovers after relaxation. Different from the PB sample which shows large breaks and fracture, the NI-80 electrode has similar surface morphologies and crack structures to the NG sample, under and after stretching (Figure 5c−h).

Unfortunately, the maintenance of stretchability and increase of total effective area are usually contradictory. For example, the NI-1100 sample has much larger effective area than the NI-80 and NI-45 samples (Figure 4a), but its critical strain is less than 60% (Figure 5a) due to further interruption of the crack expansion. As mentioned above, platinum can grow unlimitedly out of plane only occupying 25% of the electrode surface area; however, with the increasing height of nanoislands, the equivalent thickness of the SNCG film modified with nanoislands increases, thereby, according to Formula 1, the transverse wrinkle is to some extent inhibited, which may further alter the dynamic behavior of crack expansion. Given the porosity of 25% and pore size of 200 nm in this study, combined experimental data is analyzed theoretically (see detailed derivation in Supporting Information), and the semiquantitative explanation is shown in Figure 5b. As the quantity of platinum modification increases, the critical strain, ε_c, the equivalent capacitance per area, C/C_{NG}, the density of initial cracks, ρ_c, and the wavelength of wrinkles, λ_w, experience three typical regions of the initial, the transitional, and the composite stages. Initially, the density of nanocracks declines, and the wrinkle wavelength increases as the platinum nucleates (Formula S5 in the Supporting Information), leading to a decrease of critical strain as shown in Figure 5b. After the appearance of nanoislands, the density of initial cracks stays unchanged due to the limitation of porosity. Meanwhile, the wrinkle wavelength changes little because the small amount of platinum and very short nanoislands have ignorable effects on the wrinkles (Formula S5 in the Supporting Information). Therefore, the critical strain stays at plateau during this transitional stage. As more platinum deposits and grows into nanorods or nanowires with a large aspect ratio, the inhibition

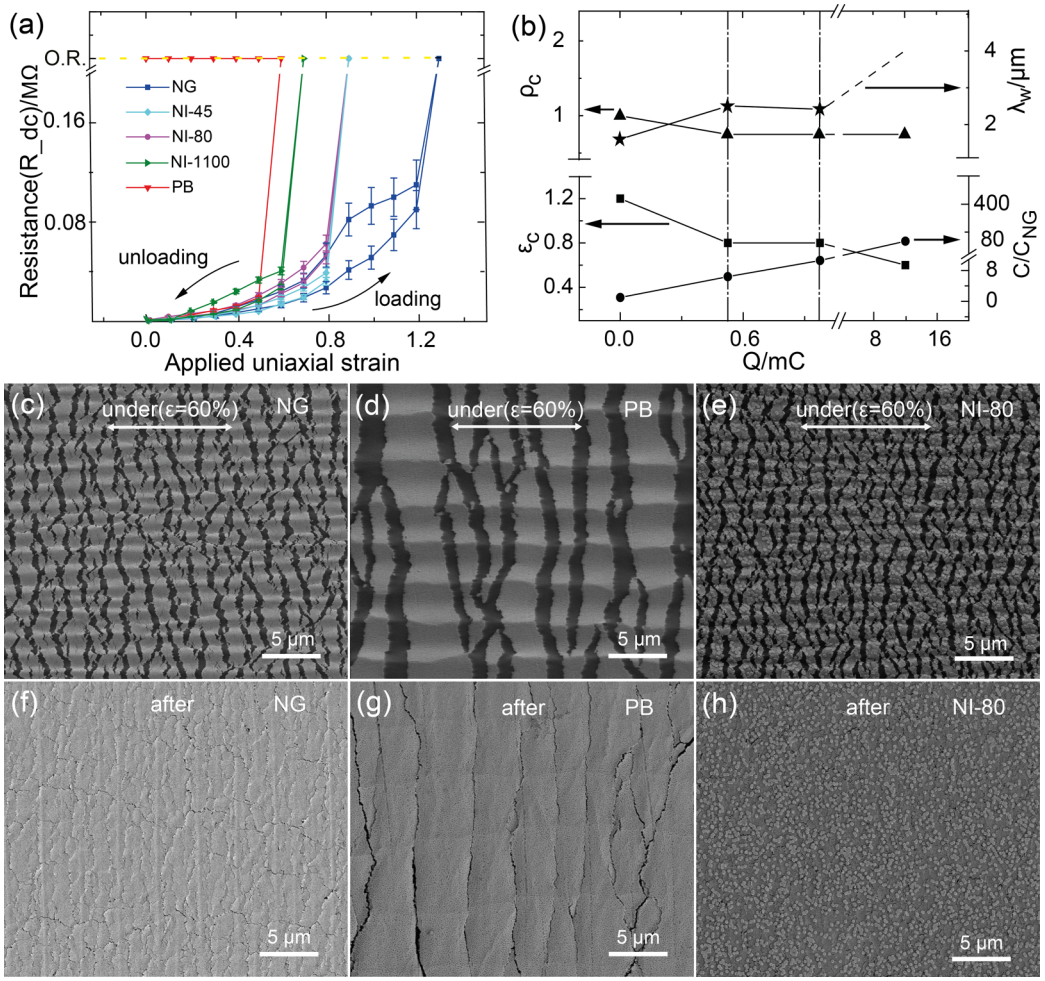

Figure 5. Comparison of the stretchability of NG (naked gold), PB (platinum black, DED 3-35), and NI-x (nano island with the height of "x" nm) electrodes and the coupling effects of multiparameters on the impedance and stretchability. (a) Resistance of the NG, PB (DED 3-35), and NI electrode while they are stretched at different applied uniaxial strains, where O.R. represents that the resistance is out of measuring range. (b) Semiquantitative analysis for the coupling effects of impedance and stretchability, where Q is the plating charge, ε_c is the critical strain, C/C_{NG} is the equivalent capacitance per area normalized by NG, ρ_c is the density of initial cracks, and λ_w is the wavelength of wrinkles. The solid line shows the experimental data, and the dashed line shows the theoretical prediction. (c–e) SEM images showing the comparison of NG, PB (DED 3-35), and NI-80 under stretching. The white double arrow lines show the direction for the uniaxial stretch. (f–h) SEM images of the corresponding samples from c to e after relaxation.

of the platinum nanoisland on transverse wrinkles becomes significant, roughly equal to the increase of film thickness. As a result, the critical strain keeps decreasing at this stage during which the wrinkles dominate. In addition, similar to Figure 4b, the equivalent capacitance keeps increasing linearly with the amount of platinum deposited or the height of nanoislands when their dispersity and diameter are fixed. In summary, for the complex structure of dispersed, porous nanoislands landing on SNCG films, the dispersity, diameter, aspect ratio, and porosity of individual nanoislands interactively affect the stretchability and electrical properties of its impedance (Figure 5b). Although the optimization of these parameters is not included in the current study, the semiquantitative analysis is provided (Formulas S4 and S5 in the Supporting Information). In detail, formula S4 describes that when the pore size and other parameters are given, the effective capacitance is linearly dependent on the height of NI, which is in accord with the experiment results shown in Figure 4b. Formula S5 describes two main factors affecting the critical strain, including the wavelength of induced wrinkles and the crack density, and the critical strain decreases with the increase of the wavelength and the decrease of the crack density, which is consistent with the experimental data shown in Figure 5b. These results demonstrate that the dispersed, porous nanoislands structure is very appropriate for the surface modification of the stretchable devices, providing controllable electrical performance and maintaining stretchability.

Additionally, we tested the stability of NI-1100 and NI-80 by applying multicycle strains with an increment of 100 cycles, a maximum strain of 20%, and a strain rate of 2% per second. For NI-1100, the equivalent capacitance changes little after 200 cycles (Figure S6b in the Supporting Information), and the conductor is not conductive after 300 cycles. We then further investigate the position of the fracture after 300 cycles by using probes (Figure S6c in the Supporting Information). The resistances between ① and ② and between ③ and ④ are conductive, but the resistance between ② and ③ is not conductive any more. In addition, the impedance of the electrode between ② and ③ is much higher, indicating that the effective area decreases dramatically. Taken together, there

must exist through cracks in the region between ② and ③, where the fracture position locates. Comparatively, the performance of NI-80 keeps stable after suffering the 300-cycle deformation (Figure S6b in the Supporting Information). This indicates that the height of nanoislands may affect the stability of SNCG films.

Further, stretchable microelectrode arrays (SMEAs) are developed with the dispersed, porous nanoislands landing on the SNCG film for monitoring intracranial electroencephalograms (EEG) or electrocorticograms (ECoG). A detailed fabrication process and the structure of SMEAs are described in the Experimental Procedures. The brain cortex has complex structures and surface morphology and is soft and vulnerable with plentiful blood vessels. Therefore, the electrodes have to conformally wrap on the cortex surface for effective communication between the brain and the electrodes. ECoG signals are continuously recorded for 90 min. During the recording sessions, neither breakage nor injurious stress to the cortex is observed, and the ECoG electrode is conformably attached on the cortex surface (Figure 6a). The impedance of

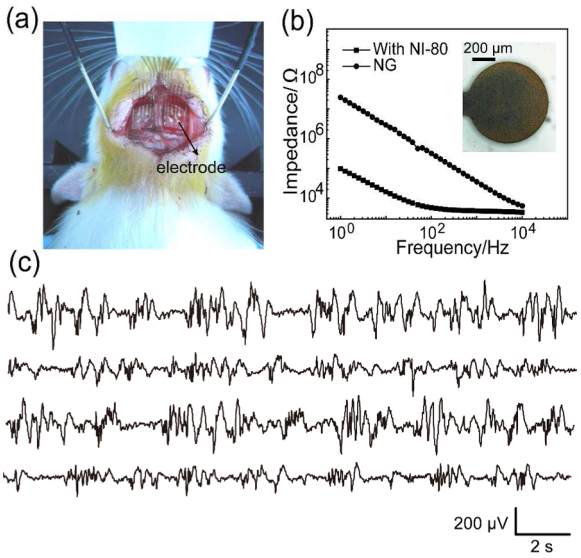

Figure 6. Intracranial EEG recording from a rat by using an SMEA developed with dispersed, porous nanoislands landing on the SNCG film. (a) An SMEA with two 2 × 2 arrays for the left and right brain hemispheres is placed on rat cortex to record intracranial EEG. (b) Impedance spectroscopy of a typical electrode in a before and after the deposition with nanoislands of NI-80. An optical photograph of the NI-80 microelectrode is shown in the inset of b. (c) Intracranial EEG signals recorded simultaneously from four of the eight microelectrodes in a are shown in c. The upper two-channel signals are recorded from the left brain hemisphere and the other two recorded from the right.

an individual microelectrode with dispersed, porous nanoislands is significantly lower than those naked SNCG microelectrodes of the same size (Figure 6b), indicating a better capability of monitoring neural signals. ECoG signals are successfully recorded with comparable SNR from multiple channels simultaneously, and the signals from four selected channels (two channels from the left brain hemisphere and the other two from the right) are shown in Figure 6c. The SNR of neural signals obtained from our electrode is about 4.58 ± 0.07 (mean ± S.D.), which is comparable with that from the commercial electrodes with an SNR of 4.67 ± 0.09 (see the details in the Supporting Information). The results indicate that the complex structure of dispersed, porous nanoislands landing on the SNCG film is well deformed with the curved surface of the brain cortex and provides an effective conformal neural-electronic interface.

3. CONCLUSION

In this study, we have fabricated stretchable nanocrack gold films that can be stretched as much as 120% uniaxial strain and maintain their electrical conductivity under stretching. The SNCG film can be bent, stretched, or twisted while keeping conductive in the presence of cracks and their dynamic expansion under tension. However, once a continuous modification layer of platinum black is plated on the SNCG film, the cross-linked platinum retards the propagation of cracks by selectively welding or fully covering the cracks. As a result, the film loses its stretchability in the end. To address this issue, we design and demonstrate that a complex structure of dispersed, porous nanoislands landing on the SNCG film can well maintain the stretchability as it allows propagation of cracks. Moreover, the total effective area, which is a key factor for its electrical performance, can be precisely controlled by modulating the dispersity, diameter, aspect ratio, and porosity of individual nanoislands. In addition, the SMEAs developed based on the complex structure of dispersed, porous nanoislands landing on the SNCG film can spread over the curved surface of the rat cortex, providing a friendly bioelectronic interface for monitoring intracranial EEG. Besides direct applications, the dispersed nanoislands landing on an SNCG film may provide a stage for various materials and structures landing with maintaining the strechability of the whole film surface. This technology overcomes the inherent limitation of using stiff and nonstrechable materials on stretchable substrates and creates a view for the development of stretchable nanoelectronic devices.

EXPERIMENTAL PROCEDURES

Fabrication of SNCG Films and Electrodes. Fabrication process of the SNCG films and electrodes was described with the schematic illustration shown in Figure S1 in the Supporting Information. A silicon wafer used as a rigid backing was coated with a monolayer of 1H, 1H, 2H, 2H perfluoro-octyl-trichlorosilane (48931-10G, Sigma-Aldrich) to facilitate the removal of silicone membranes at the end of fabrication. The silicone prepolymer and the cross-linker were mixed in a 10:1 ratio by weight (PDMS; Sylgard 184, Dow Corning), with mixing and defoaming in a conditioning mixer (AR-100, Thinky Mixer, Japan), then spun on the silicon wafer at 600 rpm for 60 s for the substrate and 800 rpm for 60 s for the encapsulation block. The PDMS was cured at 80 °C for 3 h. This preparation produced a 110-μm-thick PDMS membrane for the substrate and a 50-μm-thick PDMS membrane for encapsulation. After plasma treatment (operating in air atmosphere) on the PDMS substrate, a 3-nm-thick titanium adhesion layer followed by a 50-nm-thick gold film was deposited through a prepatterned, stainless steel mask by a direct-current (dc) magnetron sputtering system (JS4S-75G, JSWN, China). After being peeled off from the silicon wafer, the electrode sample was bonded and encapsulated with the prepared 50-μm-thick PDMS membrane. For the SNCG film conductor sample, the mask pattern was designed similar to a dumbbell: two pads at the ends were squares (1.5 mm × 1.5 mm); the wire in between was 500 μm in width and 8 mm in length. The scale marker along the wire was 150 μm in width. Following the scale markers along the wire, the PDMS encapsulation block was bonded on the substrate leaving a window of 500 μm by 1 mm in the middle exposed to be the testing electrode for modification. No obvious delamination of the metal film was found after the removal of the PDMS encapsulation (in Figure S1: the step from S1h to S1i).

As described in the previous part, the 50-μm-thick PDMS block (in Figure S1g,h) was fully cured at 80 °C for 3 h before being placed on the metal film as a temporal encapsulation layer. Therefore, there was no participation of the metal film during the curing of PDMS, and the temporal bonding between the PDMS block and the metal film was formed with the help of electrostatic force given by the high surface energy of PDMS, which could provide enough adhesion force and would not delaminate the metal film when the encapsulation block was removed manually and gently. For the SMEAs for monitoring intracranial EEG, two groups of a total eight microelectrodes were designed with 700 μm in diameter of microelectrodes and 1.5 mm interspacing between two adjacent microelectrodes. The SMEAs were packaged with flexible PCB boards for the system integration and connection to an electroencephalograph system.

Electrodeposition. The electrodepostion process includes the DED method and TAED method in this study. Both methods were performed with an electrochemical workstation (Reference 600 potentiostat, Gamry Instruments). The exposed electrode region was obliquely immersed in a working solution with a saturated calomel electrode (SCE) and a spiral platinum wire as the reference and counter electrodes. A wire with a ball at one end wrapped up with conductive Gold Paste (Pelco, Ted Pella) was prepared to form intimate electrical contact with the SNCG pad by gently touching on its surface. The working solution contained chloroplatinic acid (0.025 M H_2PtCl_6) and boric acid (0.2 m L^{-1} H_3BO_3) in DI water. The nanoisland structure was fabricated with the template of a porous polycarbonate (PC) membrane (Isopore, Millipore). The pore size was 200 nm in diameter with a porosity of 25% and an averaged thickness of 25 μm. As shown in Figure S1 in the Supporting Information, the PC membrane was attached on the SNCG film with the help of electrostatic force, and then the film was encapsulated with the prepared 50-μm-thick PDMS membrane, leaving the same exposed area as that in the DED method. After electrodeposition, the PC membrane was dissolved by a photoresist remover (Remover PG, Microchem, MA).

DC Resistance and EIS Measurement. DC resistance with different tensile strain was measured by a multimeter (17B, Fluke). The samples were gradually stretched and relaxed by a customized, manual stretcher (Figure S3c in the Supporting Information), and after each increment of strain, the resistance is measured at each static strain while holding the strain unchanged for measurement to avoid the effect of velocity. Electrochemical impedance spectrum (EIS) measurements were conducted with the same electrochemical workstation as above in phosphate buffered saline (PBS, pH 7.4) at frequencies ranging from 1 Hz to 10 kHz. The sample was stretched by a customized, manual stretcher as shown in Figure S3c and a customized, automated stretcher as shown in Figure S6a in the Supporting Information.

Animal Surgery and Intracranial EEG Recording. Adult male Sprague−Dawley rats (250−300g), obtained from Guangdong Medical Experimental Animal Center (Guangzhou, China), were used in this study. All procedures were performed in accordance with the guidelines of the Institutional Animal Care and Use Committee of Shenzhen Institutes of Advanced Technology, Chinese Academy of Sciences. A craniotomy procedure was implemented for placing the SMEA on the rat brain cortex, before which the SMEA was encapsulated by placing the PDMS block on the conducting lines with the help of a manipulation platform with optical amplifying devices exposing the detecting pads, and the rat was anesthetized with intraperitoneal injection (i.p.) of chloral hydrate (CAS No. 302-17-0, Sinopharm Chemical Reagent, China) at a dose of 350 mg/kg body weight and fixed to the stereotaxic equipment. The skin was cut near the parietal bone, two windows (a 4 × 5 mm longitudinal incision on each hemisphere of the brain) were opened on the skull by a miniature hand-held cranial drill, and the SMEA was then placed onto the cortex. The intracranial EEG was recorded with a 64-channel wireless Bluetooth video electroencephalograph system (NATION7128, Nuocheng, China) with a 128 Hz sampling rate, 60 Hz low-pass filter, and 50 Hz notch frequency. The neural recordings were performed in a shielding Faraday cage to eliminate the external electromagnetic interference.

■ ASSOCIATED CONTENT

Ⓢ Supporting Information

Supporting Information is available for additional detailed descriptions of experimental setups, parameter optimization, formula derivation, and modeling analysis. This material is available free of charge via the Internet at http://pubs.acs.org/.

■ AUTHOR INFORMATION

Corresponding Author

*Tel.: +86 (755)-86392217. Fax: +86 (755)-86392299. E-mail: zhe.yu@siat.ac.cn.

Author Contributions

‡These authors contributed equally.

Notes

The authors declare no competing financial interest.

■ ACKNOWLEDGMENTS

We acknowledge Hongzhi Zhang, Yi Lu, and Fengrui Zhou for their assistance in equipment operations and Yang Zhao for constructive discussion. This work was supported by National Natural Science Foundation of China (61374013 and 61102042) and Shenzhen "Peacock Plan" to Z.Y.

■ ABBREVIATIONS

SNCG = stretchable nanocrack gold
DED = direct electrodeposition
TAED = template-assisted electrodeposition
PB = platinum black
NG = naked gold
NI-45 = the nanoislands with a height of 45 nm
TAED 3-3600 = the current density of 3 mA/cm^2 is applied for 3600s using TAED method
O.R. = out of measuring range

■ REFERENCES

(1) Ahn, J. H.; Je, J. H. Stretchable Electronics: Materials, Architectures and Integrations. *J. Phys. D: Appl. Phys.* **2012**, *45* (10), 103001.

(2) Holtzheimer, P. E.; Kelley, M. E.; Gross, R. E.; Filkowski, M. M.; Garlow, S. J.; Barrocas, A.; Wint, D.; Craighead, M. C.; Kozarsky, J.; Chismar, R. Subcallosal Cingulate Deep Brain Stimulation for Treatment-resistant Unipolar and Bipolar Depression. *Arch. Gen. Psychiatry* **2012**, *69* (2), 150−158.

(3) Boretius, T.; Badia, J.; Pascual-Font, A.; Schuettler, M.; Navarro, X.; Yoshida, K.; Stieglitz, T. A Transverse Intrafascicular Multichannel Electrode (TIME) to Interface with The Peripheral Nerve. *Biosens. Bioelectron.* **2010**, *26* (1), 62−69.

(4) Morrison, B., III; Elkin, B. S.; Dollé, J. P.; Yarmush, M. L. In Vitro Models of Traumatic Brain Injury. *Annu. Rev. Biomed. Eng.* **2011**, *13*, 91−126.

(5) Yu, Z.; Graudejus, O.; Tsay, C.; Lacour, S. P.; Wagner, S.; Morrison, B., III. Monitoring Hippocampus Electrical Activity In Vitro on An Elastically Deformable Microelectrode Array. *J. Neurotraum.* **2009**, *26* (7), 1135−1145.

(6) Graudejus, O.; Yu, Z.; Jones, J.; Morrison, B., III; Wagner, S. Characterization of An Elastically Stretchable Microelectrode Array and Its Application to Neural Field Potential Recordings. *J. Electrochem. Soc.* **2009**, *156* (6), 85−94.

(7) Someya, T. *Stretchable Electronics*; Wiley-VCH: Birmingham, 2013.

(8) Lacour, S. P.; Jones, J.; Wagner, S.; Li, T.; Suo, Z. Stretchable Interconnects for Elastic Electronic Surfaces. *Proc. IEEE* **2005**, *93* (8), 1459−1467.
(9) Graudejus, O.; Goïrn, P.; Wagner, S. Controlling The Morphology of Gold films on Poly (dimethylsiloxane). *ACS Appl. Mater. Interfaces* **2010**, *2* (7), 1927−1933.
(10) Robinson, A. P.; Minev, I.; Graz, I. M.; Lacour, S. P. Microstructured Silicone Substrate for Printable and Stretchable Metallic Films. *Langmuir* **2011**, *27* (8), 4279−4284.
(11) Xu, S.; Zhang, Y.; Cho, J.; Lee, J.; Huang, X.; Jia, L.; Fan, J. A.; Su, Y.; Su, J.; Zhang, H. Stretchable Batteries with Self-similar Serpentine Interconnects and Integrated Wireless Recharging Systems. *Nat. Commun.* **2013**, *4*, 1543.
(12) Kim, D. H.; Xiao, J.; Song, J.; Huang, Y.; Rogers, J. A. Stretchable, Curvilinear Electronics Based on Inorganic Materials. *Adv. Mater.* **2010**, *22* (19), 2108−2124.
(13) Blau, A.; Murr, A.; Wolff, S.; Sernagor, E.; Medini, P.; Iurilli, G.; Ziegler, C.; Benfenati, F. Flexible, All-polymer Microelectrode Arrays for The Capture of Cardiac and Neuronal signals. *Biomaterials* **2011**, *32* (7), 1778−1786.
(14) Kim, K. S.; Zhao, Y.; Jang, H.; Lee, S. Y.; Kim, J. M.; Kim, K. S.; Ahn, J. H.; Kim, P.; Choi, J. Y.; Hong, B. H. Large-scale Pattern Growth of Graphene Films for Stretchable Transparent Electrodes. *Nature* **2009**, *457* (7230), 706−710.
(15) Lee, Y.; Bae, S.; Jang, H.; Jang, S.; Zhu, S. E.; Sim, S. H.; Song, Y. I.; Hong, B. H.; Ahn, J. H. Wafer-scale Synthesis and Transfer of Graphene Films. *Nano Lett.* **2010**, *10* (2), 490−493.
(16) Rogers, J. A.; Someya, T.; Huang, Y. Materials and Mechanics for Stretchable Electronics. *Science* **2010**, *327* (5973), 1603−1607.
(17) Lacour, S. P.; Chan, D.; Wagner, S.; Li, T.; Suo, Z. Mechanisms of Reversible Stretchability of Thin Metal Films on Elastomeric Substrates. *Appl. Phys. Lett.* **2006**, *88* (20), 204103.
(18) Chun, K. Y.; Oh, Y.; Rho, J.; Ahn, J. H.; Kim, Y. J.; Choi, H. R.; Baik, S. Highly Conductive, Printable and Stretchable Composite Films of Carbon Nanotubes and Silver. *Nat. Nanotechnol.* **2010**, *5* (12), 853−857.
(19) Park, M.; Im, J.; Shin, M.; Min, Y.; Park, J.; Cho, H.; Park, S.; Shim, M. B.; Jeon, S.; Chung, D. Y. Highly Stretchable Electric Circuits from A Composite Material of Silver Nanoparticles and Elastomeric Fibres. *Nat. Nanotechnol.* **2012**, *7* (12), 803−809.
(20) Kim, Y.; Zhu, J.; Yeom, B.; Di Prima, M.; Su, X.; Kim, J. G.; Yoo, S. J.; Uher, C.; Kotov, N. A. Stretchable Nanoparticle Conductors with Self-organized Conductive Pathways. *Nature* **2013**, *500* (7460), 59−63.
(21) Graudejus, O.; Morrison, B., III; Goletiani, C.; Yu, Z.; Wagner, S. Encapsulating Elastically Stretchable Neural Interfaces: Yield, Resolution, and Recording/Stimulation of Neural Activity. *Adv. Funct. Mater.* **2012**, *22* (3), 640−651.
(22) Graz, I.; Krause, M.; Bauer-Gogonea, S.; Bauer, S.; Lacour, S. P.; Ploss, B.; Zirkl, M.; Stadlober, B.; Wagner, S. Flexible Active-matrix Cells With Selectively Poled Bifunctional Polymer-ceramic Nanocomposite for Pressure and Temperature Sensing Skin. *J. Appl. Phys.* **2009**, *106* (3), 034503.
(23) Mehring, C.; Rickert, J.; Vaadia, E.; De Oliveira, S. C.; Aertsen, A.; Rotter, S. Inference of Hand Movements from Local Field Potentials in Monkey Motor Cortex. *Nat. Neurosci.* **2003**, *6* (12), 1253−1254.
(24) Brankovic, S.; Wang, J.; Adžić, R. Metal Monolayer Deposition by Replacement of Metal Adlayers on Electrode Surfaces. *Surf. Sci.* **2001**, *474* (1), L173−L179.
(25) Petrossians, A.; Whalen, J. J.; Weiland, J. D.; Mansfeld, F. Electrodeposition and Characterization of Thin-film Platinum-iridium Alloys for Biological Interfaces. *J. Electrochem. Soc.* **2011**, *158* (5), D269−D276.
(26) Negi, S.; Bhandari, R.; Rieth, L.; Solzbacher, F. In Vitro Comparison of Sputtered Iridium Oxide and Platinum-coated Neural Implantable Microelectrode Arrays. *Biomed. Mater.* **2010**, *5* (1), 015007.
(27) Kim, J. H.; Kang, G.; Nam, Y.; Choi, Y. K. Surface-modified Microelectrode Array with Flake Nanostructure for Neural Recording and Stimulation. *Nanotechnology* **2010**, *21* (8), 085303.
(28) Brüggemann, D.; Wolfrum, B.; Maybeck, V.; Mourzina, Y.; Jansen, M.; Offenhäusser, A. Nanostructured Gold Microelectrodes for Extracellular Recording From Electrogenic Cells. *Nanotechnology* **2011**, *22* (26), 265104.
(29) Baranauskas, G.; Maggiolini, E.; Castagnola, E.; Ansaldo, A.; Mazzoni, A.; Angotzi, G. N.; Vato, A.; Ricci, D.; Panzeri, S.; Fadiga, L. Carbon Nanotube Composite Coating of Neural Microelectrodes Preferentially Improves The Multiunit Signal-to-noise Ratio. *J. Neural. Eng.* **2011**, *8* (6), 066013.
(30) Cui, X.; Lee, V. A.; Raphael, Y.; Wiler, J. A.; Hetke, J. F.; Anderson, D. J.; Martin, D. C. Surface Modification of Neural Recording Electrodes with Conducting Polymer/Biomolecule Blends. *J. Biomed. Mater. Res.* **2001**, *56* (2), 261−272.
(31) Lu, Y.; Li, Y.; Pan, J.; Wei, P.; Liu, N.; Wu, B.; Cheng, J.; Lu, C.; Wang, L. Poly (3, 4-ethylenedioxythiophene)/Poly (styrenesulfonate)-poly (vinyl alcohol)/Poly (acrylic acid) Interpenetrating Polymer Networks for Improving Optrode-neural Tissue Interface in Optogenetics. *Biomaterials* **2012**, *33* (2), 378−394.
(32) Harris, A. R.; Morgan, S. J.; Chen, J.; Kapsa, R. M.; Wallace, G. G.; Paolini, A. G. Conducting Polymer Coated Neural Recording Electrodes. *J. Neural Eng.* **2013**, *10* (1), 016004.
(33) Chen, H.; Guo, L.; Ferhan, A. R.; Kim, D. H. Multilayered Polypyrrole-coated Carbon Nanotubes to Improve Functional Stability and Electrical Properties of Neural Electrodes. *J. Phys. Chem. C* **2011**, *115* (13), 5492−5499.
(34) Graudejus, O.; Jia, Z.; Li, T.; Wagner, S. Size-dependent Rupture Strain of Elastically Stretchable Metal Conductors. *Scr. Mater.* **2012**, *66* (11), 919−922.
(35) Minev, I.; Lacour, S. P. Impedance Spectroscopy on Stretchable Microelectrode Arrays. *Appl. Phys. Lett.* **2010**, *97* (4), 043707.
(36) Cyganowski, A.; Minev, I. R.; Vachicouras, N.; Musick, K.; Lacour, S. P. In *Sensors*; Chiou, J. C., Vig, J., Eds.; IEEE: Piscataway, NJ, 2012; pp 893−896.
(37) Graz, I. M.; Cotton, D. P.; Lacour, S. P. Extended Cyclic Uniaxial Loading of Stretchable Gold Thin-films on Elastomeric Substrates. *Appl. Phys. Lett.* **2009**, *94* (7), 071902.
(38) Pine, J. Recording Action Potentials From Cultured Neurons with Extracellular Microcircuit Electrodes. *J. Neurosci. Methods* **1980**, *2* (1), 19−31.
(39) Rand, D.; Woods, R. The Nature of Adsorbed Oxygen on Rhodium, Palladium and Gold Electrodes. *J. Electroanal. Chem. Interfacial Electrochem.* **1971**, *31* (1), 29−38.
(40) Huang, Z.; Hong, W.; Suo, Z. Nonlinear Analyses of Wrinkles in A Film Bonded to A Compliant Substrate. *J. Mech. Phys. Solids.* **2005**, *53* (9), 2101−2118.
(41) Tian, B.; Zheng, X.; Kempa, T. J.; Fang, Y.; Yu, N.; Yu, G.; Huang, J.; Lieber, C. M. Coaxial Silicon Nanowires as Solar Cells and Nanoelectronic Power Sources. *Nature* **2007**, *449* (7164), 885−889.
(42) Tian, B.; Xie, P.; Kempa, T. J.; Bell, D. C.; Lieber, C. M. Single-crystalline Kinked Semiconductor Nanowire Superstructures. *Nat. Nanotechnol.* **2009**, *4* (12), 824−829.
(43) Moré, J. J. In *Numerical Analysis*; Watson, J. A., Ed; Springer: New York, 1978; pp 105−116.